

## Article

# Mathematical Simulation of Heat Transfer in Thermally Magnetised Oldroyd-B Fluid in Sakiadis Rheology with a Heat Reservoir

Zeeshan <sup>1,†</sup>, Rasool Shah <sup>2</sup>, Waris Khan <sup>3</sup>, Essam R. El-Zahar <sup>4,5</sup>, Se-Jin Yook <sup>6,\*</sup> and Nehad Ali Shah <sup>7,†</sup>

<sup>1</sup> Department of Mathematics and Statistics, Bacha Khan University Charsadda, Charsadda 24420, KP, Pakistan; zeeshan@bkuc.edu.pk

<sup>2</sup> Department of Mathematics, Abdul Wali Khan University Mardan, Mardan 23200, KP, Pakistan; rasoolshah@awkum.edu.pk

<sup>3</sup> Department of Mathematics, Hazara University Mansehra, Mansehra 21120, KPK, Pakistan; dr.wariskhan@hu.edu.pk

<sup>4</sup> Department of Mathematics, College of Science and Humanities in Al-Kharj, Prince Sattam bin Abdulaziz University, P.O. Box 83, Al-Kharj 11942, Saudi Arabia; er.elzahar@psau.edu.sa

<sup>5</sup> Department of Basic Engineering Science, Faculty of Engineering, Menoufia University, Shebin El-Kom 32511, Egypt

<sup>6</sup> School of Mechanical Engineering, Hanyang University, 222 Wangsimni-ro, Seongdong-gu, Seoul 04763, Korea

<sup>7</sup> Department of Mechanical Engineering, Sejong University, 209 Neungdong-ro, Gwangjin-gu, Seoul 05006, Korea; nehadali199@sejong.ac.kr

\* Correspondence: ysjnuri@hanyang.ac.kr

† These authors contributed equally to this work and are co-first authors.



**Citation:** Zeeshan; Shah, R.; Khan, W.; El-Zahar, E.R.; Yook, S.-J.; Shah, N.A. Mathematical Simulation of Heat Transfer in Thermally Magnetised Oldroyd-B Fluid in Sakiadis Rheology with a Heat Reservoir. *Mathematics* **2022**, *10*, 1775. <https://doi.org/10.3390/math10101775>

Academic Editors: Mingheng Li and Hui Sun

Received: 17 April 2022

Accepted: 17 May 2022

Published: 23 May 2022

**Publisher's Note:** MDPI stays neutral with regard to jurisdictional claims in published maps and institutional affiliations.



**Copyright:** © 2022 by the authors. Licensee MDPI, Basel, Switzerland. This article is an open access article distributed under the terms and conditions of the Creative Commons Attribution (CC BY) license (<https://creativecommons.org/licenses/by/4.0/>).

**Abstract:** Sakiadis rheology of a generalised polymeric material, as well as a heat source or sink and a magnetic field, are all part of this study. Thermal radiations have been introduced into the convective heating process. The translation of a physical situation into a set of nonlinear equations was achieved through mathematical modelling. To convert the resulting partial differential equation into a set of nonlinear ordinary differential equations, appropriate transformations have been used. The velocity and temperature profiles are generated both analytically by HAM and numerically by the Runge–Kutta method (RK-4). In order to analyse the behaviour of the physical quantities involved, numerical and graphical depictions have been offered. To show that the acquired findings are correct, a nonlinear system error analysis has been offered. The heat flux study has been shown using bar charts. For the essential factors involved, the local Nusselt number and local Skin friction are calculated in tabular form. The fluid particles' molecular mobility was slowed due to the magnetic field and porosity, and the heat transfer rates were demonstrated to be lowered when magnetic and porosity effects are present. This magnetic field and porosity effects regulating property has applications in MHD ion propulsion and power production, the electromagnetic casting of metals, etc. Furthermore, internal heat absorption and generation have diametrically opposed impacts on fluid temperature. The novelty of the present study is that no one has investigated the Sakiadis flow of thermal convection magnetised Oldroyd-B fluid in terms of a heat reservoir across a porous sheet. In limited circumstances, a satisfactory match is revealed when the collected values are compared to the existing work published corroborating the current attempt. The findings of this study are expected to be applicable to a wide range of technical and industrial processes, including steel extrusion, wire protective layers, fiber rolling, fabrication, polythene stuff such as broadsheet, fiber, and stainless steel sheets, and even the process of depositing a thin layer where the sheet is squeezed.

**Keywords:** numerical solution; heat reservoir; thermal performance; MHD flow; Sakiadis flow

**MSC:** 80A05

## 1. Introduction

Flow field problems influenced by sliding surfaces with convective heat transfer underneath the implementation of magnetic properties (MHD) are one of the beneficial challenges in computational fluid dynamics because of their significance with designing and manufacturing—for example, in steel extrusion, wire protective layers, fiber rolling, pultrusion, fabrication, polythene stuff (e.g., broadsheet, fiber, and stainless steel sheets), and even in the procedure of depositing a thin layer where the sheet undergoes the squeezing occurrence [1–5]. The value of the ultimate output in these applications is greatly influenced by the cooling rate; therefore, in these operations, the mechanism of the cooling rate leads to the desired final product [6,7]. Sakiadis [8,9] discusses significant work on boundary layer flows and effectively applies it to a variety of applications in industry and engineering. Scholars in the fields of applied mathematics and physics later looked into his theories and used them to solve a variety of new scientific challenges, such as Zierep and Fetecau [10], who looked into the Rayleigh–Stokes problem involving the Maxwell fluid. Jamil et al. [11] used the unsteady helical flow of fluid to solve fluidics problems. They reported the relaxation/retardation time features of the Oldroyd-B fluid model. Tan and Masuoka [12] provided stability assessments for the problem of Maxwell fluid in porous media with thermal heating. Nadeem et al. [13] analysed the boundary layer flow towards a stretched sheet in the vicinity of the stagnation point using Homotopy. Hayat et al. [14] estimated thermal radiation and Joule heating dynamics using Oldroyd-B fluid for MHD flow in the thermophoresis phenomena circumstances. Malik et al. [15] investigated the three-dimensional mixed convective flow problem dynamics with an upper-convective Maxwell fluid and magnetic field, whereas Hayat et al. [16] investigated the mixed convective three-dimensional flow problem dynamics with a magnetic field and an upper-convective Maxwell fluid. Mehmood et al. [17] reported a numerical approach for micropolar Casson fluid over a stretched sheet. Ramesh et al. [18] explored the problem of heat generation in nanofluid flow on Maxwell fluid. Mehmood et al. [19] investigated the Jeffery micro fluid impinging obliquely on a stretched plate. Kumar [20] calculated the thermal radiation impact on the flow of Oldroyd B nanofluid. Rana et al. [21] offered a numerical approach to the case of non-linear thermal radiation problems for non-Newtonian flow. Awais et al. [22] studied the polymeric nanofluid's Sakiadis flow, and, in general, several studies [23–27] have recently been presented to examine the physical behaviour of fluid mechanics problems, and references have been made in them.

The purpose of this research is to examine the fluid flow across a moving surface in new ways. The heat transmission for the flow of Sakiadis was analysed for the rheology of an Oldroyd-B fluid. The presence of a generalised magnetic field term is revealed through mathematical modelling of the momentum equation. The fluid dynamics in a porous medium are investigated using internal heat absorption or generation as well as thermal radiation effects. Analytical and numerical treatments for momentum and energy dynamics have been carried out using HAM and RK-4, respectively [28–36].

Barman et al. [37] studied the magnetised bi-convective nanomaterial with base fluid properties using temperature-sensitive base, and a unique solution has been obtained. Ghalambaz et al. [38] explored the melting performance of PCMs in a hollow focus to a non-uniform magnetic field with a grid technique. Rehman et al. [39] investigated the numerical solution of multiple slip influence on the magnetised Casson fluid dispersed nanomaterial. The analytical solution of chemically Casson fluid flow with joule heating and a temperature dependent viscosity effect has been carried out by Rasheed et al. [40].

To demonstrate the validity of the acquired data, the velocity and temperature profiles are subjected to an error analysis. In terms of numbers and graphs, the effect of rheology on the physical quantities involved is studied using tables and charts. The novelty of the present study is that no one has investigated the Sakiadis flow of thermal convection magnetised Oldroyd-B fluid in terms of a heat reservoir across a porous sheet. When the collected data are compared to previous values, a satisfactory match is achieved in restricted cases, confirming the current effort. This study's conclusions should be applicable to a

wide range of technical and industrial operations, such as steel extrusion, wire protective layers, fiber rolling, fabrication, polythene stuff (e.g., broadsheet, fiber, and stainless steel sheets), and even in the procedure of depositing a thin layer where the sheet undergoes the squeezing occurrence.

**2. Mathematical Formulation**

Consider the Oldroyd-B model rheology (a sort of fluid model that is based on rates) when it passes through a wall. Within a porous medium, the Sakiadis flow condition has been considered. To forecast magneto-hydrodynamics, a transverse magnetic field of intensity  $B_0$  is supplied, as illustrated in Figure 1. The thermal characteristics at the wall and within the system have been studied using the convective heat process. The flow with internal heat generation/absorption qualities is governed by mathematical formulae.

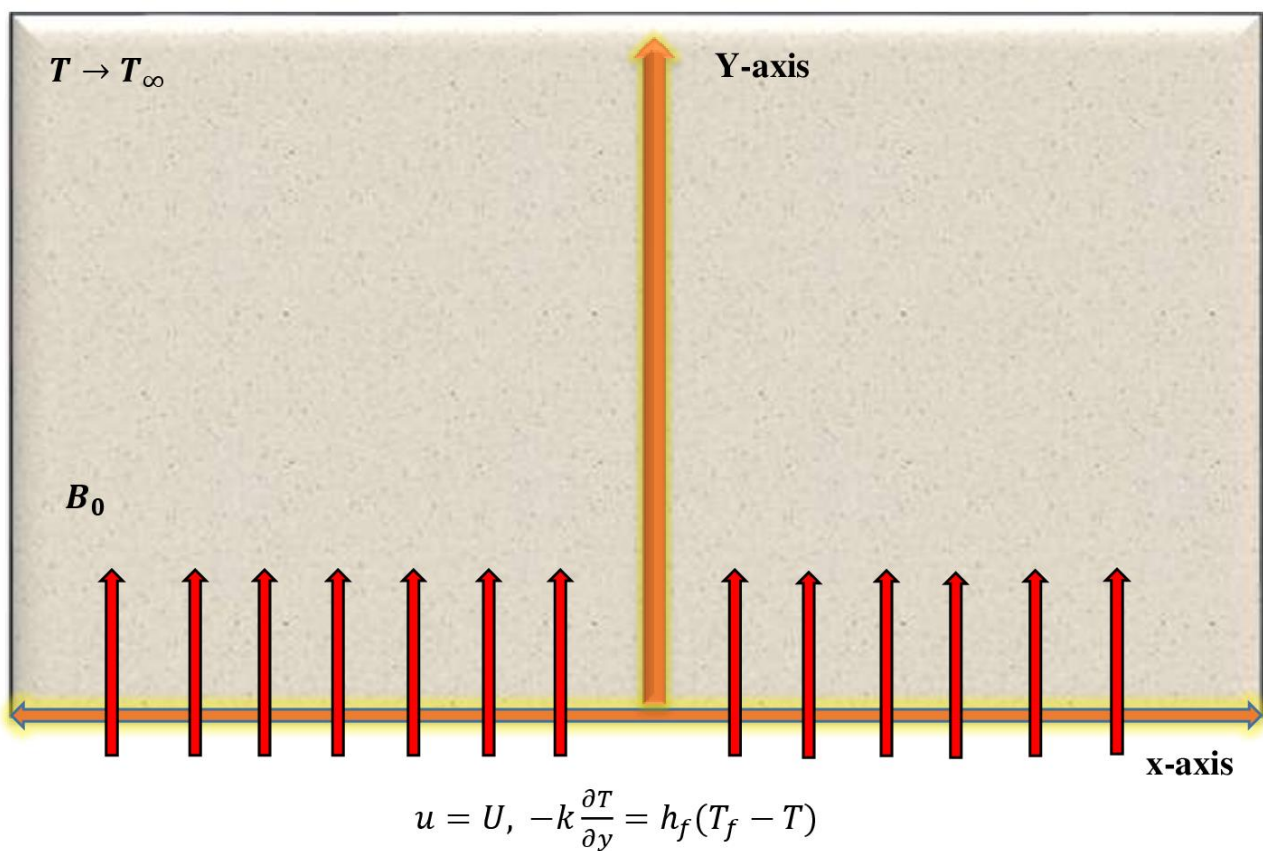


Figure 1. Geometry of the physical model [3,11,13,14,22,32–36].

$$\frac{\partial u}{\partial x} + \frac{\partial v}{\partial y} = 0 \tag{1}$$

$$\begin{aligned} \rho \left( \frac{\partial u}{\partial t} + u \frac{\partial u}{\partial x} + v \frac{\partial u}{\partial y} \right) &= -\frac{\partial p}{\partial x} + \mu \left( \frac{\partial^2 u}{\partial x^2} + \frac{\partial^2 u}{\partial y^2} \right) - \sigma B_0^2 u \\ \rho \left( \frac{\partial v}{\partial t} + u \frac{\partial v}{\partial x} + v \frac{\partial v}{\partial y} \right) &= -\frac{\partial p}{\partial y} + \mu \left( \frac{\partial^2 v}{\partial x^2} + \frac{\partial^2 v}{\partial y^2} \right) - \sigma B_0^2 v \end{aligned} \tag{2}$$

$$\left( 1 + \zeta_1 \frac{DS}{Dt} \right) = \eta + \eta \zeta_2 \left( \frac{DA_1}{Dt} \right), \tag{3}$$

$$\frac{Da_i}{Dt} - \frac{\partial a_i}{\partial t} - u_r a_{i,r} + u_{i,r} a_r = 0 \tag{4}$$

$$\rho C_p \left( \frac{\partial \theta}{\partial t} + u \frac{\partial \theta}{\partial x} + v \frac{\partial \theta}{\partial y} \right) = k \left( \frac{\partial^2 \theta}{\partial x^2} + \frac{\partial^2 \theta}{\partial y^2} \right) + q_r \tag{5}$$

here, the  $u$  and  $v$  signify the velocity components,  $\rho$  stands for the density of the fluid,  $S$  is the stress tensor,  $A_1$  denotes the Rivlin–Ericksen tensor,  $\zeta_1$  is the relaxation time effect,  $\zeta_2$  represents the retardation time effect,  $\eta$  is the dynamic viscosity, and  $D/Dt$  is the covariant derivative.

From Equations (2)–(5) we have:

$$u \frac{\partial u}{\partial x} + v \frac{\partial u}{\partial y} = -\zeta_1 \left( u^2 \frac{\partial^2 u}{\partial x^2} + v^2 \frac{\partial^2 u}{\partial x^2} + 2uv \frac{\partial^2 u}{\partial y \partial x} \right) - \left( \frac{\sigma B_0^2 u}{\rho} + \frac{v}{k} \right) \left( u + \zeta_1 v \frac{v}{k} \right) + v \left[ \frac{\partial^2 u}{\partial y^2} + \zeta_2 \left( u \frac{\partial^2 u}{\partial y^2 \partial x} + v \frac{\partial^3 u}{\partial y^3} - \frac{\partial u}{\partial x} \frac{\partial^2 u}{\partial y^2} - \frac{\partial u}{\partial y} \frac{\partial^2 v}{\partial y^2} \right) \right] \tag{6}$$

$$u \frac{\partial \theta}{\partial x} + v \frac{\partial \theta}{\partial y} = \alpha_m \frac{\partial^2 \theta}{\partial y^2} - \frac{1}{\rho C_p} \frac{\partial q_r}{\partial y} + \frac{Q_0}{\rho C_p} (\theta - \theta_\infty) \tag{7}$$

The related BC are [22]

$$\begin{aligned} u = U_w, v = 0, -k \frac{\partial \theta}{\partial y} = h_f (\theta_f - \theta), & \quad \text{at } y = 0 \\ u \rightarrow 0, v \rightarrow 0, \theta \rightarrow \theta_\infty & \quad \text{at } y \rightarrow \infty \end{aligned} \tag{8}$$

It is worth noting that for  $\zeta_2 = 0$ , the Maxwell model can be obtained. Furthermore, in the case of  $\zeta_1 = \zeta_2 = 0$ , a Newtonian fluid model is obtained. In the above equation,  $\sigma$  and  $\theta$  indicate the fluid’s conductivity and heating rate, respectively. Moreover,  $B_0, K, c_p, \alpha_m$ , and  $Q_0$  are the magnetic field strength, material porosity, heat capacity constancy, thermal conductivity, and inner heat permeation/absorption parameter, respectively, whereas the radiation thermal transit amount  $q_r$  is described as  $q_r = -(4\sigma^3/3k) \frac{\partial \theta^4}{\partial y}$ .

Using the transformation listed below [3,4],

$$\eta = \left( \frac{U_w}{\nu x} y \right)^{1/2}, u = U_w \zeta', v = -1/2 \left( \frac{v U_w}{x} y \right)^{1/2} (\zeta - \eta \zeta'), T(\eta) = \frac{\theta - \theta_\infty}{\theta_f - \theta_\infty} \tag{9}$$

Hence, Equations (5)–(8) become

$$\begin{aligned} \zeta''' + \left( \frac{1}{2} \right) \zeta \zeta'' - \frac{D_1}{2} (2\zeta \zeta' \zeta'' + \eta \zeta'^2 \zeta'' + \zeta^2 \zeta''') - M^2 (\zeta' - D_1 (\zeta - \eta \zeta') \zeta'') \\ - K \zeta' + K D_1 (\zeta \zeta'' - \eta \zeta' \zeta'') + D_2 (2(\eta \zeta' \zeta''' + \eta \zeta' \zeta'''' - \zeta' \zeta'''')) - \zeta \zeta^{iv} - \zeta''^2 = 0 \end{aligned} \tag{10}$$

$$T'' + Pr \left( \frac{1}{2} \zeta T' + h_s T \right) + \frac{4}{3} R_d T'' = 0 \tag{11}$$

$$\begin{aligned} \zeta(\eta) = 0, \zeta'(\eta) = 1, T'(\eta) = -1(1 - T(\eta)), & \quad \text{at } \eta = 0 \\ \zeta'(\eta) \rightarrow 0, T(\eta) \rightarrow 0 & \quad \text{at } \eta = \infty \end{aligned} \tag{12}$$

In Equation (10),  $D_1$  and  $D_2$  are the Deborah numbers,  $M$  is the magnetic field, and  $K$  is the porosity parameter. In Equation (11),  $Pr$  is the Prandtl number,  $h_s$  is the heat source parameter, and  $R_d$  is the thermal radiation parameter, which is defined as:

$$\begin{aligned} D_1 = \frac{\zeta_1 U}{2x}, D_2 = \frac{\zeta_2 U}{2x}, M^2 = \frac{\sigma B_0^2}{\rho U}, K = \frac{v}{kU}, R_d = \frac{16\sigma\theta_\infty^3}{3k^*k^*}, \\ Pr = \frac{v}{\alpha_m}, h_s = \frac{Q_0}{\rho C_p U}. \end{aligned}$$

The physical quantity of interest is the thermal radiation, and the wall is given by

$$Nu = \frac{xq_x}{k(\theta_\zeta - \theta_\infty)} \tag{13}$$

where

$$q_w = -k \left( \frac{\partial \theta}{\partial y} \right)_{y=0} + (q_r)_{y=0} \tag{14}$$

In dimensionless form, we have

$$Nu_x/Re^{1/2} = -\left(1 + \frac{4}{3}R_d\right)T'(0) \tag{15}$$

In Equations (14) and (15),  $q_w$  and  $Re$  denote the wall heat flux and Reynolds number, respectively.

### 3. Numerical Procedure and Validation

The forward, backward, and central difference method was developed in order to obtain the numerical solution for the system of nonlinear higher order differential equations. For this goal, the ODEs are first converted to first order ODEs by using a suitable transformation along with boundary conditions. Then, they are solved by the RK-4 built-in function in MATLAB [38–41]. The Shooting technique is used to integrate a definite value for  $h$ . If the right step size  $Dh$  is chosen, this technique contains a procedure for calculating the solution. At each stage, two different solution estimations are generated and assessed. The assumption is approved if the two answers are close; otherwise, the step size is reduced until the desired precision is achieved. We utilised a  $Dh = 0.01$  step size and accuracy to the fifth decimal point for this project. Figure 2 shows the flow chart for the numerical system.

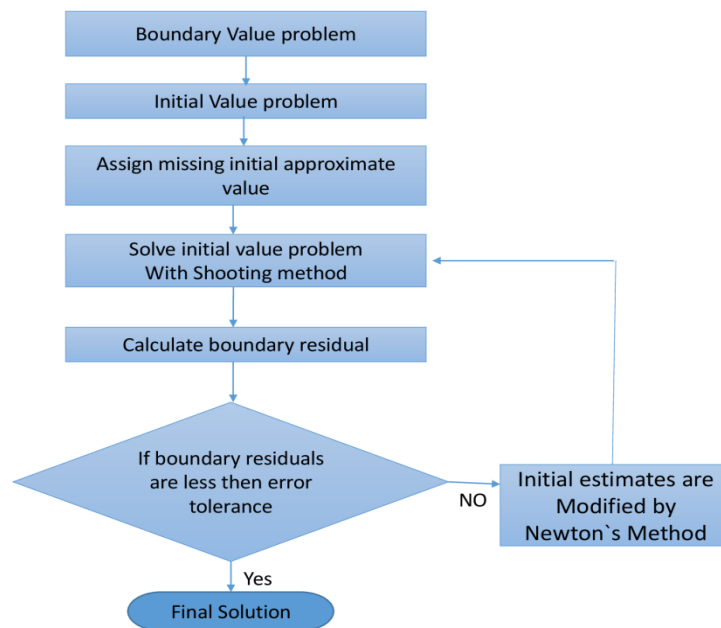


Figure 2. Flow diagram of the numerical procedure.

Equations (10) and (11) and boundary condition (12) are extremely nonlinear and interconnected. As a consequence, the error analysis was carried out in order to obtain the confirmed data. The code is also validated using Bvph2, and great agreement is found. The confirmation of two approaches, RK-4 and bvph2, as well as the CPU time up to the 10th iteration order, is shown in Table 1. As seen in this table, the computation error is rather small. Additionally, the residual error of RK-4 and bvph2 is also given in tabular form for the velocity and temperature profiles. Table 2 shows the comparison of the RK-4 and bvph2, which clarifies that the precision is comparatively insignificant for the velocity profile. The current study is compared to the published work reported by Gireesha et al. [3] for additional confirmation, and good agreement is discovered, as shown in Table 3. Figures 3 and 4 show the validity of these two approaches as well. Similarly, for the temperature profile, the validation of RK-4 and bvph2 is given in Table 4.

**Table 1.** RK-4 and bvph2 evaluations for 20th order approximation with CPU time.

<b>m</b>	<b>bvph2</b>	<b>RK-4</b>	<b>CPU Time (s)</b>
2	$3.1 \times 10^{-6}$	$1.3 \times 10^{-4}$	1.179692
3	$3.0 \times 10^{-8}$	$2.7 \times 10^{-5}$	5.9045437
4	$4.9 \times 10^{-10}$	$6.71 \times 10^{-6}$	20.1231686
5	$6.9 \times 10^{-12}$	$2.1 \times 10^{-6}$	50.4153629
6	$1.5 \times 10^{-13}$	$8.8 \times 10^{-7}$	110.9415963
7	$2.4 \times 10^{-15}$	$4.4 \times 10^{-7}$	217.3541494
8	$6.0 \times 10^{-17}$	$2.4 \times 10^{-7}$	404.8458581
9	$1.1 \times 10^{-18}$	$1.5 \times 10^{-7}$	716.4912224
10	$2.8 \times 10^{-20}$	$9.1 \times 10^{-8}$	1213.6447644
20	$5.3 \times 10^{-22}$	$5.7 \times 10^{-8}$	2262.5860728

**Table 2.** Validation of RK-4 and bvph2 for the velocity field.

<b><math>\eta</math></b>	<b>RK-4</b>	<b>bvph2</b>	<b>Absolute Error</b>
0	1.000000	1.000000	$1.110220 \times 10^{-16}$
0.5	0.661166	0.660837	0.000330
1.0	0.425501	0.424831	0.000670
1.5	0.266090	0.265040	0.001050
2.0	0.162121	0.160630	0.001491
2.5	0.096694	0.094680	0.002014
3.0	0.056780	0.054141	0.002639
3.5	0.033032	0.029642	0.003390
4.0	0.019178	0.014881	0.004297
4.5	0.011226	0.005830	0.005396
5.0	0.006738	$-1.046940 \times 10^{-7}$	0.006738

**Table 3.** Validation of the present work and the published work reported by Giresha et al. [22].

<b><math>\eta</math></b>	<b>Present Work</b>	<b>Published Work [3]</b>
0	1.000000	1.000000
0.5	0.661166	0.661163
1.0	0.425501	0.425502
1.5	0.266090	0.266094
2.0	0.162121	0.162120
2.5	0.096694	0.096693
3.0	0.056780	0.056781
3.5	0.033032	0.033034
4.0	0.019178	0.019175
4.5	0.011226	0.011223
5.0	0.006738	0.006739

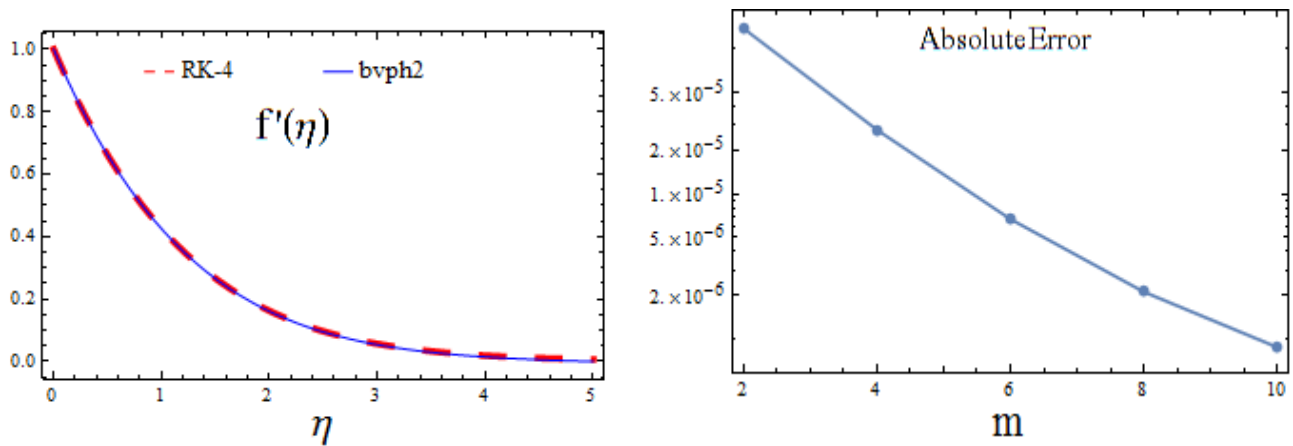


Figure 3. Validation and error analysis for the velocity profile.

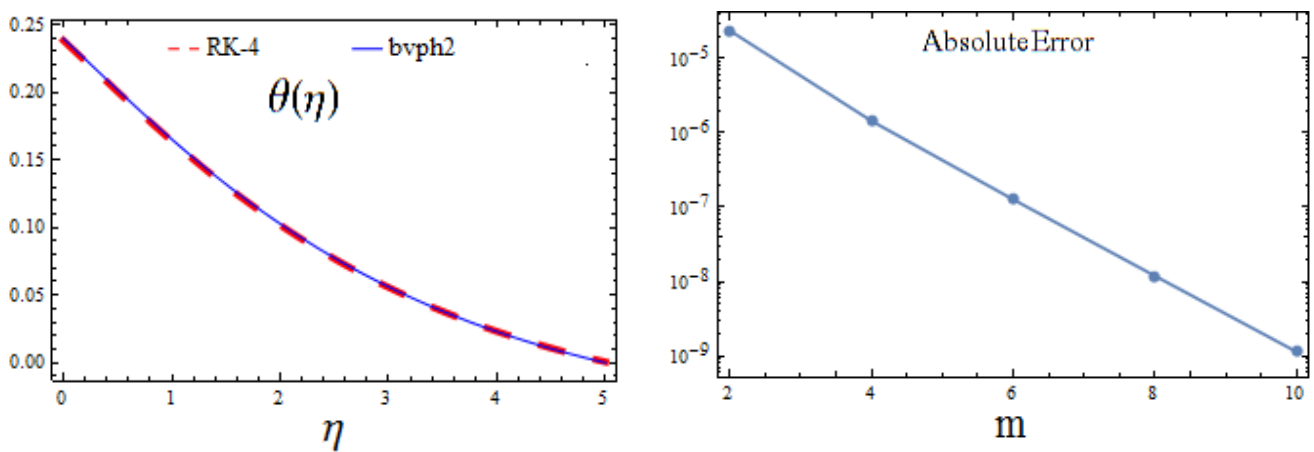


Figure 4. Temperature profile validation and error analysis.

Table 4. Validation of RK-4 and bvph2 for the temperature field.

$\eta$	RK-4	bvph2	Absolute Error
0	0.238311	0.239864	0.001553
0.5	0.200323	0.201763	0.001441
1.0	0.163895	0.165234	0.001339
1.5	0.130803	0.131982	0.001179
2.0	0.101765	0.102711	0.000947
2.5	0.076819	0.077492	0.000674
3.0	0.055675	0.056063	0.000388
3.5	0.037915	0.038021	0.000107
4.0	0.023095	0.022934	0.000160
4.5	0.010787	0.010385	0.000401
5.0	0.000613	$3.023300 \times 10^{-10}$	0.000613

#### 4. Results and Discussion

It should be emphasised that the wall convection parameter, internal generation or absorption quantity of heat, magnetic parameter, Deborah numbers, and other physical and rheological parameters are all included in the system of nonlinear equations

(Equations (10)–(12)). As a result, we have created Figures 5–12. For different magnetic parameter  $M$  values, the heat transfer rate is shown in Figure 5. The findings of propane are displayed in the front red bar, while the results of ethylene glycol are displayed in the green bar. When the magnetic is raised, the heat transfer rate drops in both cases. The Deborah numbers ( $D_1$  and  $D_2$ ) influence the flow field, as illustrated in Figures 6 and 7. As the Deborah number  $D_1$  increases, the thickness of the boundary layer and the velocity profile both decrease, but as the Deborah number  $D_2$  increases, the velocity profile declines. Deborah numbers with small values ( $D_1, D_2 \ll 1$ ) represent flowing behaviour, whereas those with large values ( $D_1, D_2 \gg 1$ ) represent solid-like activity. Furthermore, the velocity profile shows an opposite trend for positive  $D_1$  and  $D_2$  values. Figure 8 illustrates the velocity profile's dependence on the magnetic field  $M$ . The magnetic parameter and the fluid velocity have an inverse relationship, as we have seen. The temperature profiles of the magnetic parameter  $M$  for various magnitudes are shown in Figure 9. The temperature and thermal boundary layer thickness improves as the magnetic parameter  $M$  increases. It is clear that the velocity of fluid and the velocity boundary layer shrink with enhancing  $M$  for both fluids. This is due to the fact that the magnetic field is normal to the fluid's direction, as the magnetic force in an opposite direction of the flow leads to an increase in the absorption of stationary fluid on the wedge and declines the speed of the flow. Therefore, the flow becomes heavier and needs further time to move. Moreover, the velocity boundary layer is thicker in the case of non-Newtonian fluid compared to Newtonian fluid. The temperature profile is illustrated in Figure 10 with the internal heat absorption or generation parameter  $hs$  influence. Figures 10 and 11 demonstrate the influence of the internal heat generation/absorption parameter  $hs$  on the temperature profile. Heat absorption is represented by  $hs < 0$ , whereas heat generation is represented by  $hs > 0$ . The temperature and its associated boundary layer appear to be dropping as a function of the heat absorption coefficient, whereas the temperature appears to be increasing in the case of heat generation. Figure 12 depicts the temperature profile variation for various Biot number  $\gamma_1$  values. For large values of  $\gamma_1$ , the temperature and thermal boundary layer thickness show a rising pattern. The most diversity may be seen near the moving wall, where the stream weakens gradually and tends to a uniform free stream.

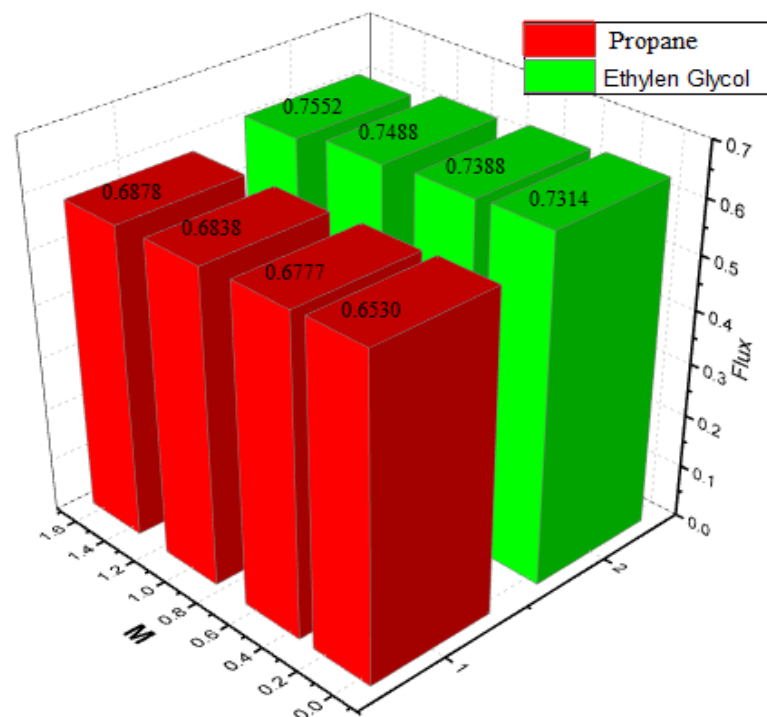


Figure 5. Impact of  $M$  on the heat transfer rate.

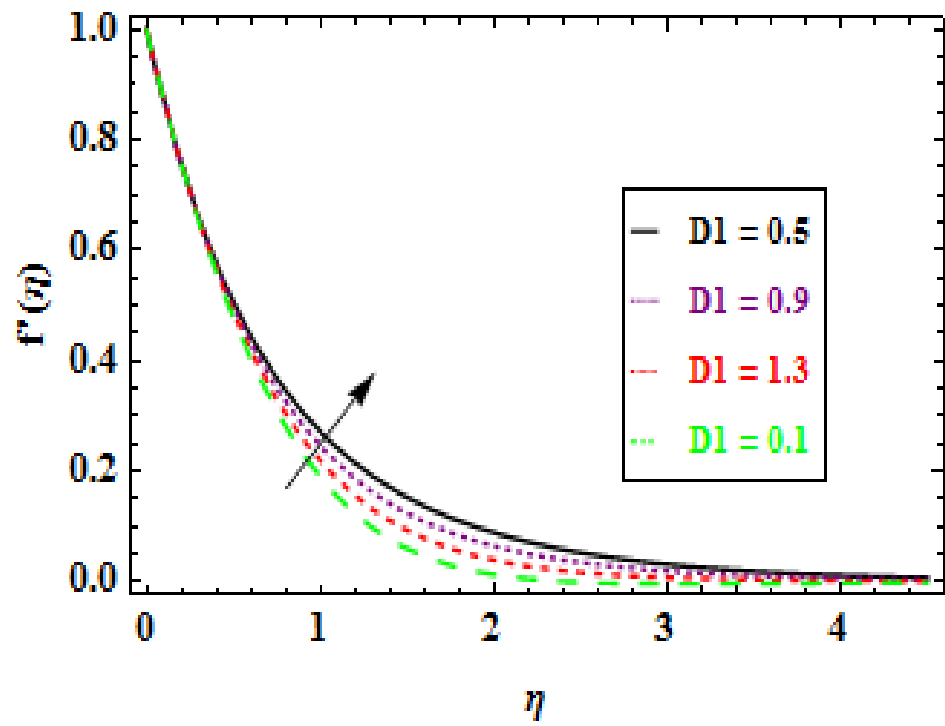


Figure 6. Impact of  $D_1$  on the velocity field.

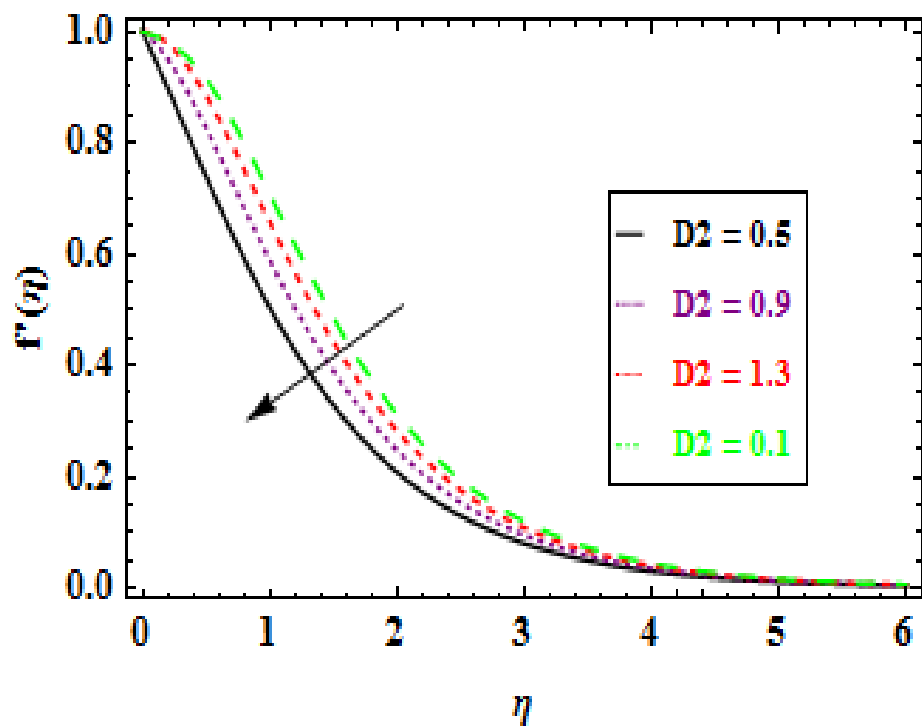


Figure 7. Impact of  $D_2$  on the velocity field.

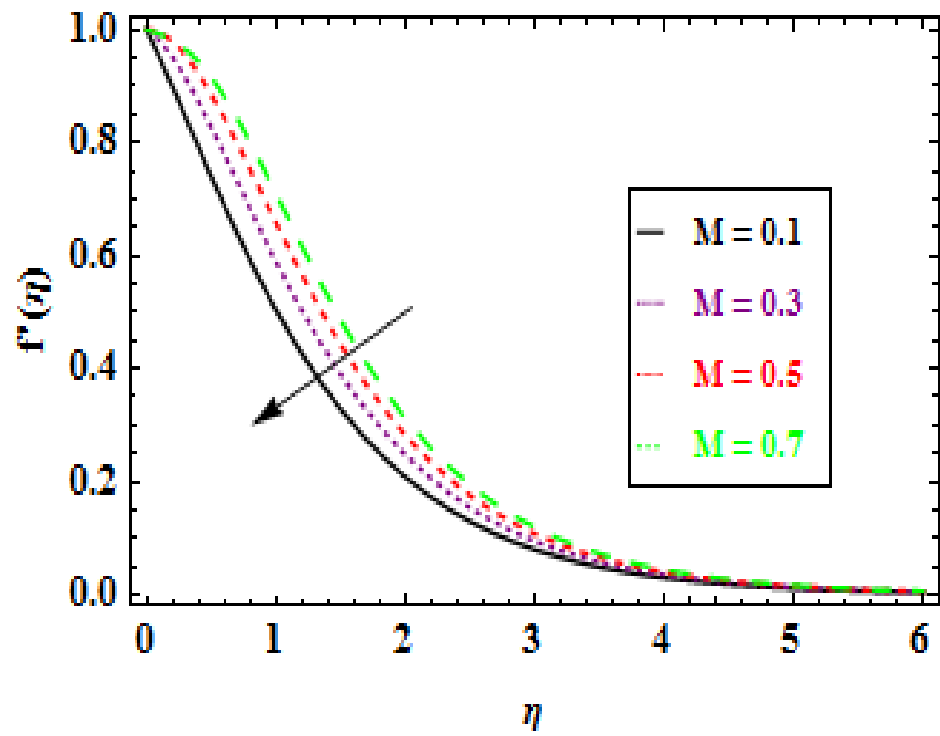


Figure 8. Impact of  $M$  on the velocity field.

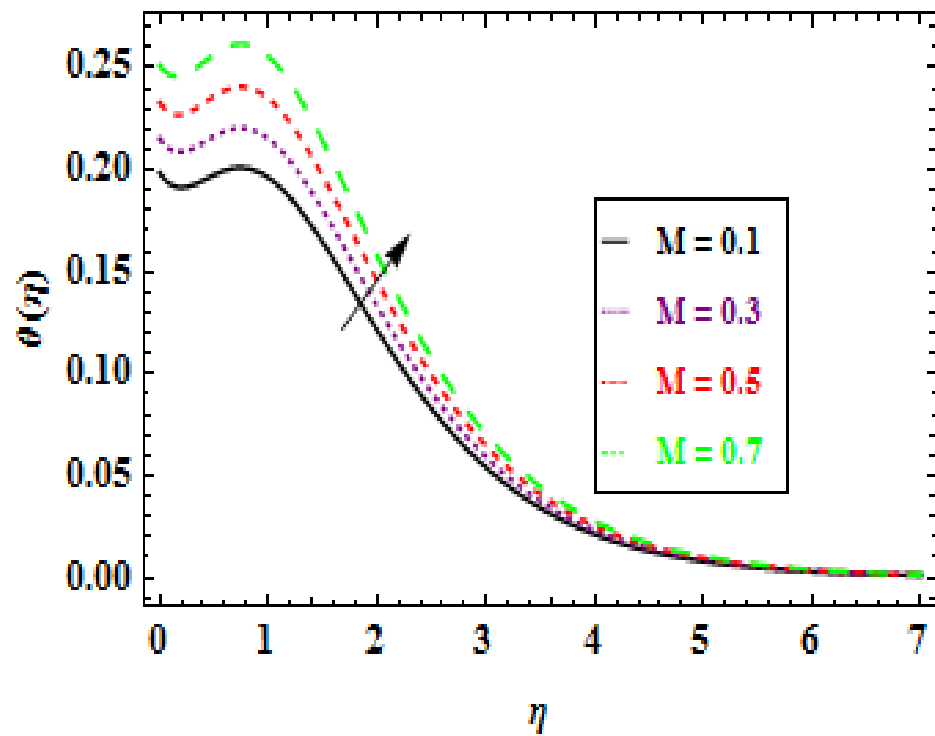


Figure 9. Impact of  $M$  on the temperature field.

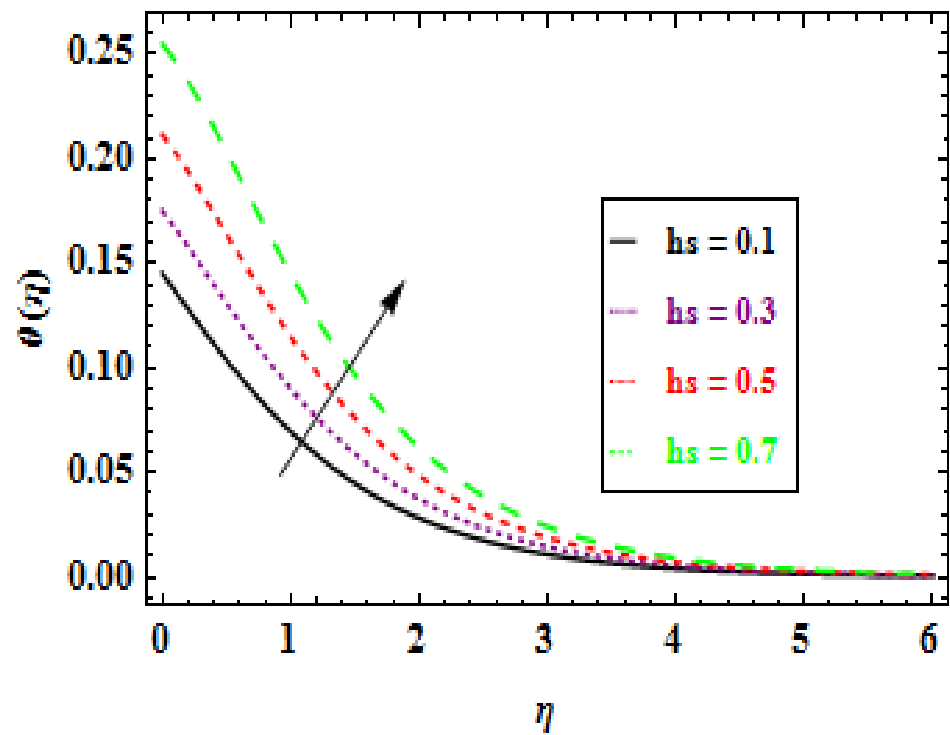


Figure 10. Impact of  $h_s$  (positive values) on the temperature field.

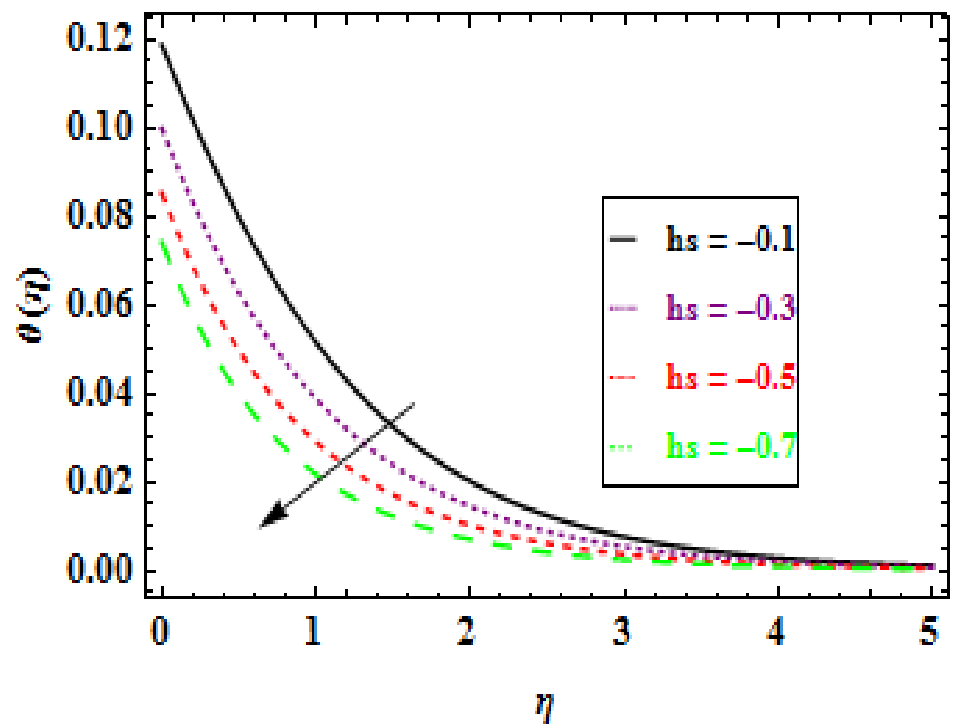


Figure 11. Impact of  $h_s$  (negative values) on the temperature field.

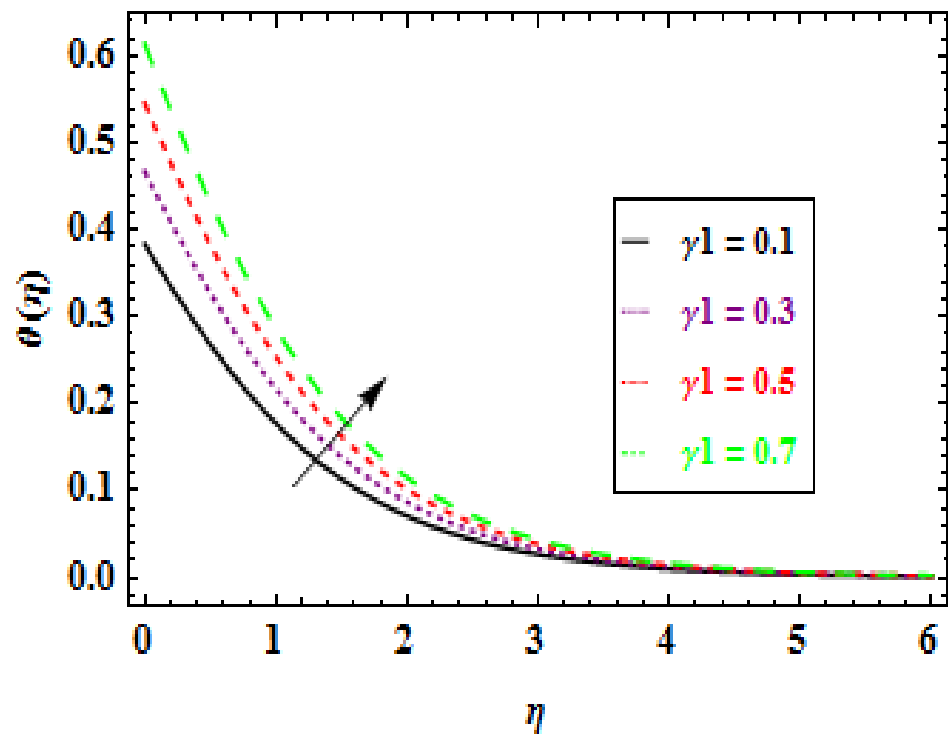


Figure 12. Impact of  $\gamma_1$  on the temperature field.

The quantitative magnitudes of local skin friction and local Nusselt numbers versus numerous rheological parameters are presented in Figures 13–17 (3D graphs) and Tables 5–21. Figure 13 represents the influence of  $D_1$  and  $M$  on the local skin friction. From this study, it is analysed that the skin friction enhances as the  $D_1$  and  $M$  are enhanced. This is due to the Lorentz force, which resists the flow and increases the local skin friction. For various values of  $D_2 = 0.1, 0.4, 1.1,$  and  $1.5$ , the variation in  $-\zeta''(0)$  is investigated, as shown in Figure 14. It is perceived that the skin friction rises with the increasing values of  $D_2$ . Similarly, investigation has been observed in Figure 15.

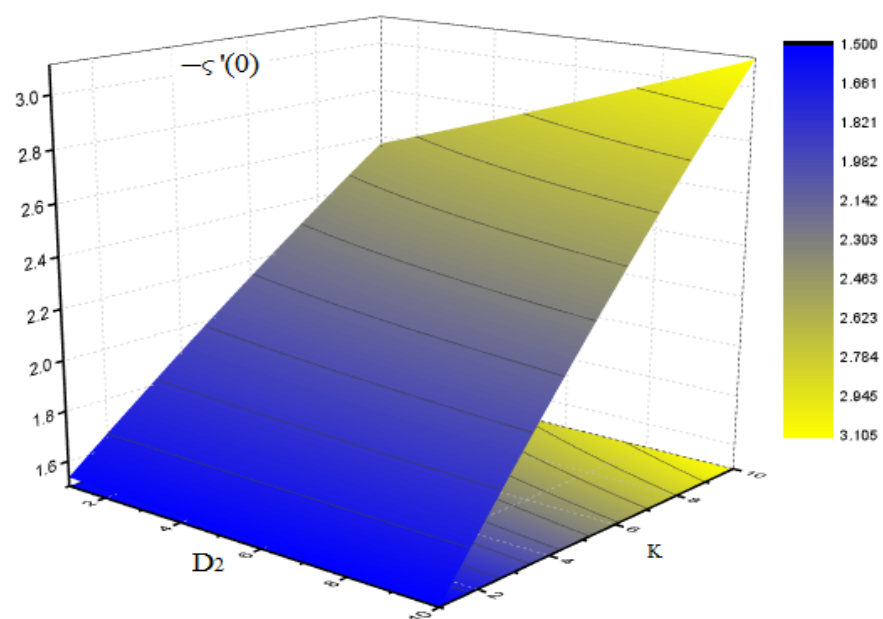


Figure 13. Skin friction variation of  $D_2$  and  $K$ .

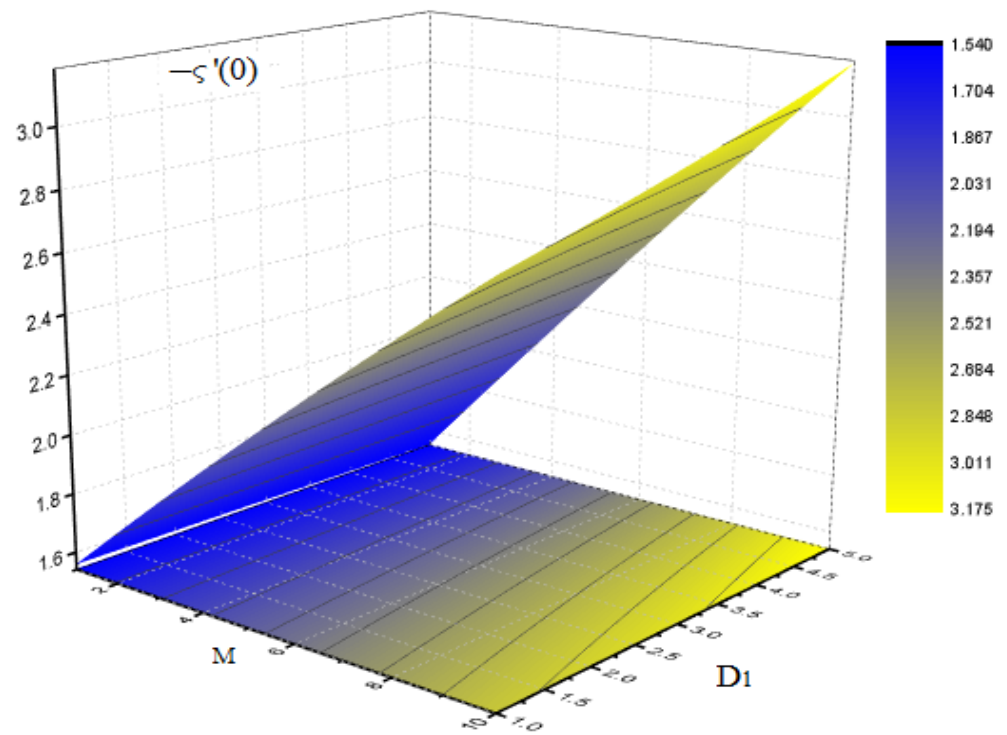


Figure 14. Skin friction variation of  $D_2$  and  $K$ .

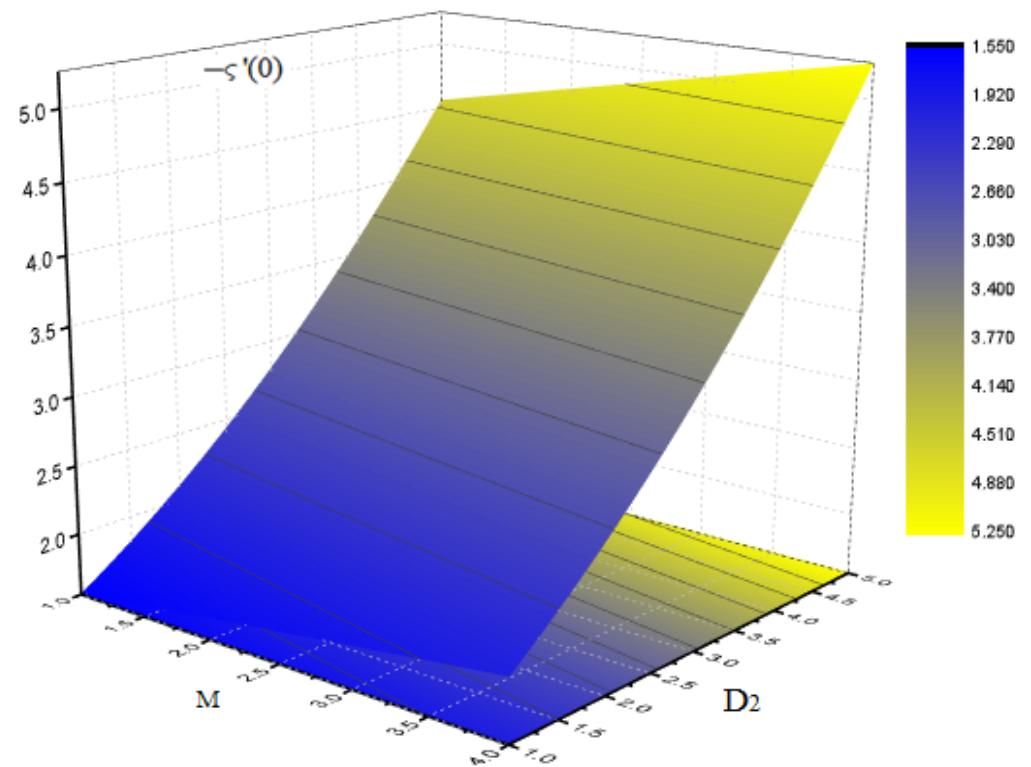


Figure 15. Skin friction variation of  $D_1$  and  $M$ .

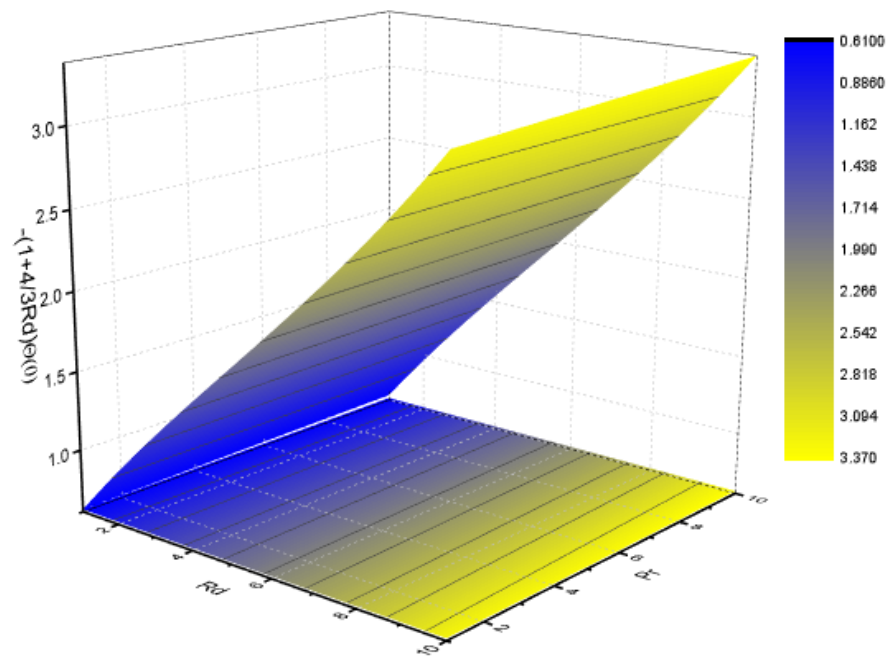


Figure 16. Skin friction variation of  $D_2$  and  $M$ .

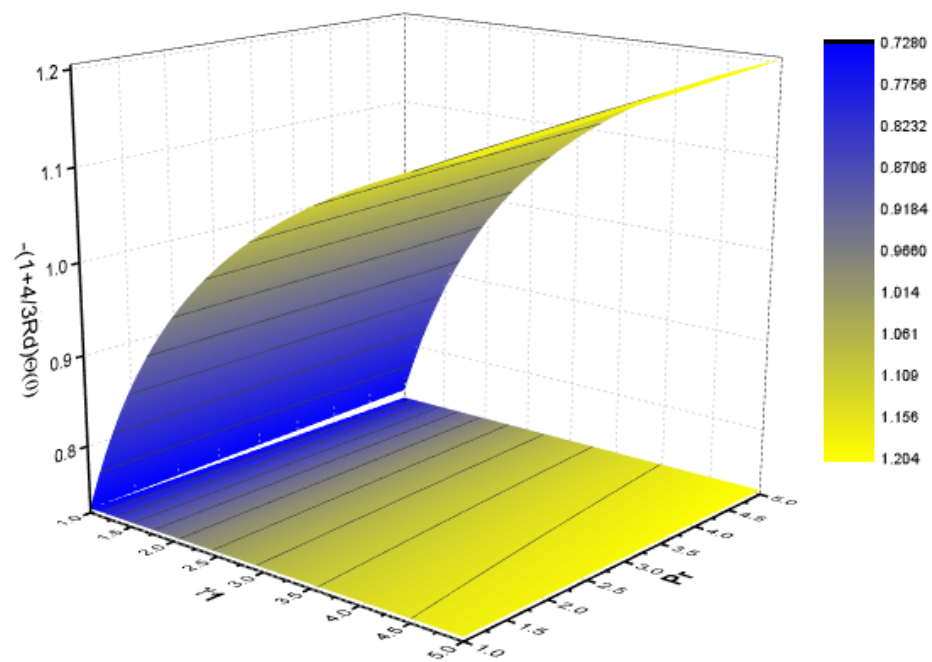


Figure 17. Nusselt number variation of  $R_d$  and  $Pr$ .

Table 5. Influence of  $D_1$  on  $-\zeta''(0)$ .

Parameters							Numerical Solutions
$D_1$	$hs$	$M$	$D_2$	$Pr$	$K$	$\gamma_1$	$-\zeta''(0)$
0.0	0.3	1	0.3	5.0	0.3	0.3	1.827825
0.3	0.3	1	0.3	5.0	0.3	0.3	1.884447
1.2	0.3	1	0.3	5.0	0.3	0.3	2.147765
1.6	0.3	1	0.3	5.0	0.3	0.3	2.215865

**Table 6.** Influence of  $hs$  on  $-\zeta''(0)$ .

Parameters							Numerical Solutions
$D_1$	$hs$	$M$	$D_2$	$Pr$	$K$	$\gamma_1$	$-\zeta''(0)$
0.3	-1.3	1	0.3	5.0	0.3	0.3	1.884447
0.3	-1	1	0.3	5.0	0.3	0.3	1.884447
0.3	-0.3	1	0.3	5.0	0.3	0.3	1.884458

**Table 7.** Influence of positive  $hs$  on  $-\zeta''(0)$ .

Parameters							Numerical Solutions
$D_1$	$hs$	$M$	$D_2$	$Pr$	$K$	$\gamma_1$	$-\zeta''(0)$
0.3	0	1	0.3	5.0	0.3	0.3	1.884431
0.3	0.4	1	0.3	5.0	0.3	0.3	1.884440
0.3	1.0	1	0.3	5.0	0.3	0.3	1.884440
0.3	1.3	1	0.3	5.0	0.3	0.3	1.885916

**Table 8.** Influence of  $M$  on  $-\zeta''(0)$ .

Parameters							Numerical Solutions
$D_1$	$hs$	$M$	$D_2$	$Pr$	$K$	$\gamma_1$	$-\zeta''(0)$
0.3	0.3	0	0.3	5.0	0.3	0.3	1.366983
0.3	0.3	0.2	0.3	5.0	0.3	0.3	1.571414
0.3	0.3	0.8	0.3	5.0	0.3	0.3	1.884441
0.3	0.3	1.5	0.3	5.0	0.3	0.3	2.458771

**Table 9.** Influence of  $D_2$  on  $-\zeta''(0)$ .

Parameters							Numerical Solutions
$D_1$	$hs$	$M$	$D_2$	$Pr$	$K$	$\gamma_1$	$-\zeta''(0)$
0.3	0.3	1	0	5.0	0.3	0.3	1.414718
0.3	0.3	1	0.4	5.0	0.3	0.	1.884432
0.3	0.3	1	1.1	5.0	0.3	0.3	4.277341
0.3	0.3	1	1.5	5.0	0.3	0.3	10.97555

**Table 10.** Influence of  $Pr$  on  $-\zeta''(0)$ .

Parameters							Numerical Solutions
$D_1$	$hs$	$M$	$D_2$	$Pr$	$K$	$\gamma_1$	$-\zeta''(0)$
0.3	0.3	1	0.3	2	0.3	0.3	1.884461
0.3	0.3	1	0.3	4	0.3	0.3	1.884461
0.3	0.3	1	0.3	6	0.3	0.3	1.884460
0.3	0.3	1	0.3	8	0.3	0.3	1.884460

**Table 11.** Influence of  $K$  on  $-\zeta''(0)$ .

Parameters							Numerical Solutions
$D_1$	$hs$	$M$	$D_2$	$Pr$	$K$	$\gamma_1$	$-\zeta''(0)$
0.3	0.3	1	0.3	5.0	0.0	0.3	1.763755
0.3	0.3	1	0.3	5.0	0.4	0.3	1.884419
0.3	0.3	1	0.3	5.0	1.2	0.3	2.358429
0.3	0.3	1	0.3	5.0	1.6	0.3	2.586296

**Table 12.** Influence of  $\gamma_1$  on  $-\zeta''(0)$ .

Parameters							Numerical Solutions
$D_1$	$hs$	$M$	$D_2$	$Pr$	$K$	$\gamma_1$	$-\zeta''(0)$
0.3	0.3	1	0.3	5.0	0.3	0.2	1.884441
0.3	0.3	1	0.3	5.0	0.3	0.6	1.884441
0.3	0.3	1	0.3	5.0	0.3	1.2	1.884441

**Table 13.** Influence of  $D_1$  on the wall temperature.

Parameters							Numerical Solutions
$D_1$	$hs$	$M$	$D_2$	$Pr$	$K$	$\gamma_1$	$(1+\frac{4}{3}R_d)T'(0)$
0.0	0.5	1.0	0.5	1.0	0.5	0.5	0.88626087
0.5	0.5	1.0	0.5	1.0	0.5	0.5	0.87047844
1.0	0.5	1.0	0.5	1.0	0.5	0.5	0.85857029
1.5	0.5	1.0	0.5	1.0	0.5	0.5	0.84965734

**Table 14.** Influence of  $hs$  (negative) on the wall temperature.

Parameters							Numerical Solutions
$D_1$	$hs$	$M$	$D_2$	$Pr$	$K$	$\gamma_1$	$(1+\frac{4}{3}R_d)T'(0)$
0.5	-1.5	1.0	0.5	1.0	0.5	0.5	0.47848456
0.5	-1	1.0	0.5	1.0	0.5	0.5	0.44917061
0.5	-0.5	1.0	0.5	1.0	0.5	0.5	0.39803006

**Table 15.** Influence of  $hs$  (positive) on the wall temperature.

Parameters							Numerical Solutions
$D_1$	$hs$	$M$	$D_2$	$Pr$	$K$	$\gamma_1$	$(1+\frac{4}{3}R_d)T'(0)$
0.5	0	1.0	0.5	1.0	0.5	0.5	0.25191604
0.5	0.5	1.0	0.5	1.0	0.5	0.5	0.35714342
0.5	1.0	1.0	0.5	1.0	0.5	0.5	0.72566043
0.5	1.5	1.0	0.5	1.0	0.5	0.5	0.87047844

**Table 16.** Influence of  $M$  on the wall temperature.

Parameters							Numerical Solutions
$D_1$	$hs$	$M$	$D_2$	$Pr$	$K$	$\gamma_1$	$(1+\frac{4}{3}R_d)T'(0)$
0.5	0.5	0.0	0.5	1.0	0.5	0.5	0.96221819
0.5	0.5	0.5	0.5	1.0	0.5	0.5	0.92237457
0.5	0.5	1.0	0.5	1.0	0.5	0.5	0.87047844
0.5	0.5	1.3	0.5	1.0	0.5	0.5	0.85099774

**Table 17.** Influence of  $D_2$  on the wall temperature.

Parameters							Numerical Solutions
$D_1$	$hs$	$M$	$D_2$	$Pr$	$K$	$\gamma_1$	$(1+\frac{4}{3}R_d)T'(0)$
0.5	0.5	1.0	0	1.0	0.5	0.5	-0.01897348
0.5	0.5	1.0	0.5	1.0	0.5	0.5	0.87047844
0.5	0.5	1.0	1.0	1.0	0.5	0.5	0.84028696
0.5	0.5	1.0	1.5	1.0	0.5	0.5	0.82674776

**Table 18.** Influence of  $Pr$  on the wall temperature.

Parameters							Numerical Solutions
$D_1$	$hs$	$M$	$D_2$	$Pr$	$K$	$\gamma_1$	$(1+\frac{4}{3}R_d)T'(0)$
0.5	0.5	1.0	0.5	0.1	0.5	0.5	0.15693718
0.5	0.5	1.0	0.5	0.5	0.5	0.5	-0.44869951
0.5	0.5	1.0	0.5	1.0	0.5	0.5	0.87047844
0.5	0.5	1.0	0.5	1.5	0.5	0.5	0.52974335

**Table 19.** Influence of  $K$  on the wall temperature.

Parameters							Numerical Solutions
$D_1$	$hs$	$M$	$D_2$	$Pr$	$K$	$\gamma_1$	$(1+\frac{4}{3}R_d)T'(0)$
0.5	0.5	1.0	0.5	1.0	0.0	0.5	0.21824554
0.5	0.5	1.0	0.5	1.0	0.5	0.5	0.87047844
0.5	0.5	1.0	0.5	1.0	1.0	0.5	0.85515317
0.5	0.5	1.0	0.5	1.0	1.5	0.5	0.84547170

**Table 20.** Influence of  $\gamma_1$  on the wall temperature.

Parameters							Numerical Solutions
$D_1$	$hs$	$M$	$D_2$	$Pr$	$K$	$\gamma_1$	$(1+\frac{4}{3}R_d)T'(0)$
0.5	0.5	1.0	0.5	1.0	0.5	0.1	0.14570719
0.5	0.5	1.0	0.5	1.0	0.5	0.5	0.87047844
0.5	0.5	1.0	0.5	1.0	0.5	1.0	2.30145457
0.5	0.5	1.0	0.5	1.0	0.5	1.5	5.09132362

**Table 21.** Comparison of non-Newtonian and Newtonian ( $\xi_1 = \xi_2 = 0$ ) fluids.

$\eta$	Non-Newtonian	Newtonian
0	1.000000	1.000000
0.5	0.661166	0.661167
1.0	0.425501	0.425512
1.5	0.266090	0.266005
2.0	0.162121	0.162100
2.5	0.096694	0.096687
3.0	0.056780	0.056780
3.5	0.033032	0.033034
4.0	0.019178	0.019179
4.5	0.011226	0.011230
5.0	0.006738	0.006740

Tables 5–7 represent the variation of  $D_1$ ,  $hs$  (for positive and negative), and  $M$  on the local skin friction. The influence of the Deborah number  $D_1$  on the skin friction is depicted in Table 5. From this analysis, it is observed that the skin friction increases as the  $D_1$  enhances. Tables 6 and 7 show that  $hs$  ( $hs > 0$  (heat generation) and  $hs < 0$  (heat absorption)) has no significant effect on the  $-\zeta''(0)$ . It is observed that  $-\zeta''(0)$  enhances as the magnetic parameter increases. This is due to the Lorentz force, which resists the flow and increases the local skin friction, as shown in Table 8. Tables 9–12 show the influence of the physical parameters  $D_2$ ,  $Pr$ ,  $K$ , and  $\gamma_1$  on the skin friction. For various values of  $D_2 = 0.1, 0.4, 1.1,$  and  $1.5$ , the variation in  $-\zeta''(0)$  is investigated. It is perceived that the skin friction rises with the increasing values of  $D_2$ , as shown in Table 9. The ratio of momentum diffusivity to heat diffusivity is described by  $Pr$ , a dimensionless quantity. This number contrasts the effects of the viscosity and heat conductivity of a fluid. The sort of fluid we are looking at is determined by the  $Pr$  number. High thermal conductivity and low  $Pr$  values characterise the heat-transmitting fluids. As seen in Table 10, raising the  $Pr$  number has little impact on skin friction and has no discernible effect. Similarly, raising the value of  $K$  in Table 11 enhances the impact. The non-dimensional heat generation/absorption parameter  $\gamma_1$  relies on the quantity of heat created by or absorbed in the fluid, and its impact on the skin friction is comparable to that of  $Pr$ , as shown in Table 12.

Tables 13–20 display the variation of the Nusselt number for numerous values of the physical parameters  $D_1$ ,  $hs$  (both positive and negative),  $M$ ,  $D_2$ ,  $Pr$ ,  $K$ , and  $\gamma_1$ . Table 13 depicts the effect of  $D_1$  on the Nusselt number. It is detected that the Nusselt number enhances as  $D_1$  is increased. The variation of  $hs$  ( $hs > 0$  (heat generation),  $hs < 0$  (heat absorption)) on the Nusselt number is indicated in Tables 14 and 15. It is predicted that the Nusselt number increases for  $hs > 0$  and declines for  $hs < 0$ , respectively. The demonstration of the Nusselt number for the physical parameters  $M$ ,  $D_2$ ,  $Pr$ , and  $\gamma_1$  on the Nusselt number is shown in Tables 16–20. It is perceived that the Nusselt number drops for the increasing values of the physical parameters  $M$ ,  $D_2$ , and  $Pr$ . The ratio of momentum diffusivity to heat diffusivity is introduced by this dimensionless variable. This number contrasts the effects of the viscosity and heat conductivity of a fluid. The  $Pr$  number indicates the type of fluid being evaluated. High thermal conductivity and low  $Pr$  values characterise heat-transmitting fluids. As seen in Table 18, the Prandtl number has little effect on the skin friction but boosts the Nusselt number. Likewise, the porosity has an increasing impact and the Biot number has a decreasing influence on the Nusselt number, as shown in Tables 19 and 20, respectively. Additionally, a comparison of the Newtonian and non-Newtonian fluid for various values of the magnetic parameter  $M$  is given in Table 21 in the revised manuscript.

The combined effects of the physical parameters  $D_1$ ,  $D_2$ ,  $K$ , and  $M$  on the skin friction are presented Figures 13–15. The parameters have a good influence on the skin friction. The influence of the Physical Parameters  $Pr$ ,  $R_d$ , and  $\gamma_1$  on the Nusselt number is presented in Figures 16 and 17. These influences are already discussed separately in the above figures.

## 5. Conclusions

In this study, the fluid flows across a permeable wall with Sakiadis Oldroyd-B dynamics were investigated. The following are some of the study's final outcomes, which are based on the graphical results:

- The velocity and momentum boundary layers diminish as the Deborah number  $D_1$  increases, but both improve as the Deborah number  $D_2$  increases.
- The Lorentz force, which resists the flow, reduces the velocity of the fluid as the magnetic parameter increases.
- By strengthening the magnetic field, the temperature profile rises.
- Over the temperature profile, opposite behaviours of heat generation and absorption effects are found.
- The temperature rises when the Biot number is high.
- From this analysis, it is observed that the skin friction increases as the  $D_1$  enhances.
- It is observed that  $-\zeta''(0)$  enhances as the magnetic parameter increases. This is due to the Lorentz force, which resists the flow and increases the local skin friction.
- Heat conducting fluids have significant thermal conductivity and a low Prandtl number, but raising the  $Pr$  has little effect on the skin friction.
- It is predicted that the Nusselt number increases for  $hs > 0$  and declines for  $hs < 0$ , respectively.
- In the future, exploring the potential stochastic numerical computing approaches using the procedures of Artificial Intelligence to analyse the Sakiadis flow dynamics of Oldroyd-B fluid via a porous wall model is intriguing.

**Author Contributions:** Data curation, E.R.E.-Z.; Formal analysis, W.K.; Methodology, R.S.; Project administration, N.A.S.; Resources, W.K.; Software, N.A.S.; Validation, E.R.E.-Z. and S.-J.Y.; Writing—original draft, Z.; Writing—review & editing, S.-J.Y. All authors have read and agreed to the published version of the manuscript.

**Funding:** This research received no external funding.

**Institutional Review Board Statement:** Not Applicable.

**Informed Consent Statement:** Not Applicable.

**Data Availability Statement:** The numerical data used to support the findings of this study are included within the article.

**Conflicts of Interest:** The authors declare no conflict of interest.

## Nomenclature

$u, v$	Velocities components
$\rho$	Density of fluid
$S$	Stress tensor
$\zeta_1$	Relaxation time
$k$	Porosity parameter
$R_d$	Thermal radiation
$\zeta_2$	Retardation time
$A_1$	Rivlin–Erickson tensor
$\mu$	Dynamic viscosity
$D/Dt$	Convective derivative
$Pr$	Prandtl number
$q_w$	Wall heat

$\sigma$	Fluid conductivity
$\theta$	Heating rate
$D_1, D_2$	Deborah numbers
$M$	Magnetic parameter
$h_s$	Heat source
$Re$	Reynolds number

## References

- Jie, P.; Ke-Qin, Z.; Bao-Shu, X. Characteristics of Electrorheological Fluid Flow Between Two Concentric Cylinders. *Chin. Phys. Lett.* **2000**, *17*, 298–300. [\[CrossRef\]](#)
- Daniel, Y.S.; Aziz, Z.A.; Ismail, Z.; Salah, F. Effects of thermal radiation, viscous and Joule heating on electrical MHD nanofluid with double stratification. *Chin. J. Phys.* **2017**, *55*, 630–651. [\[CrossRef\]](#)
- McDonald, M.; Shenkman, L. Nonlinear convective heat and mass transfer of Oldroyd-B nanofluid over a stretching sheet in the presence of uniform heat source/sink. *Results Phys.* **2018**, *9*, 1555–1563.
- Ganesh Kumar, K.; Gireesha, B.J.; Ramesh, G.K. Thermal analysis of generalized Burgers nanofluid over a stretching sheet with nonlinear radiation and non-uniform heat source/sink. *Arch. Thermodyn.* **2018**, *2*, 39.
- Shah, N.A.; Wakif, A.; El-Zahar, E.R.; Ahmad, S.; Yook, S.J. Numerical simulation of a thermally enhanced EMHD flow of a heterogeneous micropolar mixture comprising (60%)-ethylene glycol (EG), (40%)-water (W), and copper oxide nanomaterials (CuO). *Case Stud. Therm. Eng.* **2020**, 102046, In Press. [\[CrossRef\]](#)
- Colangelo, G.; Favale, E.; Milanese, M.; de Risi, A.; Laforgia, D. Cooling of electronic devices: Nanofluids contribution. *Appl. Therm. Eng.* **2017**, *127*, 421–435. [\[CrossRef\]](#)
- Gusain, R.; Khatri, O.P. Ultrasound assisted shape regulation of CuO nanorods in ionic liquids and their use as energy efficient lubricant additives. *J. Mater. Chem. A* **2013**, *1*, 5612–5619. [\[CrossRef\]](#)
- Sakiadis, B.C. Boundary-layer behavior on continuous solid surfaces: I. Boundary-layer equations for two-dimensional and axisymmetric flow. *AIChE J.* **1961**, *7*, 26–28. [\[CrossRef\]](#)
- Sakiadis, B.C. Boundary-layer behavior on continuous solid surfaces: II. The boundary layer on a continuous flat surface. *AIChE J.* **1961**, *7*, 221–225. [\[CrossRef\]](#)
- Zierep, J.; Fetecau, C. Energetic balance for the Rayleigh–Stokes problem of a Maxwell fluid. *Int. J. Eng. Sci.* **2007**, *45*, 617–627. [\[CrossRef\]](#)
- Jamil, M.K.; Fetecau, C.; Imran, M. Unsteady helical flows of Oldroyd-B fluids. *Commun. Nonlinear Sci. Numer. Simul.* **2011**, *16*, 1378–1386. [\[CrossRef\]](#)
- Tan, W.; Masuoka, T. Stability analysis of a Maxwell fluid in a porous medium heated from below. *Phys. Lett. A* **2007**, *360*, 454–460. [\[CrossRef\]](#)
- Nadeem, S.; Hussain, A.; Khan, M. HAM solutions for boundary layer flow in the region of the stagnation point towards a stretching sheet. *Commun. Nonlinear Sci. Numer. Simul.* **2010**, *15*, 475–481. [\[CrossRef\]](#)
- Hayat, T.; Alsaedi, A. On thermal radiation and Joule heating effects on MHD flow of an Oldroyd-B fluid with thermophoresis. *Arab. J. Sci. Eng.* **2011**, *36*, 1113–1124. [\[CrossRef\]](#)
- Malik, M.Y.; Farzana, R.A. Magnetohydrodynamic three-dimensional Maxwell fluid flow towards a horizontal stretched surface with convective wall. *Int. J. Bio. Engng. Life Sci.* **2015**, *2*, 211–229.
- Hayat, T.; Awais, M.; Obaidat, S. Mixed convection three-dimensional flow of an upper-convected Maxwell (UCM) Fluid under magnetic field, thermal-diffusion and diffusion-thermo effects. *ASME J. Heat Transfer* **2012**, *134*, 044503. [\[CrossRef\]](#)
- Mehmood, Z.; Mehmood, R.; Iqbal, Z. Numerical Investigation of Micropolar Casson Fluid over a Stretching Sheet with Internal Heating. *Commun. Theor. Phys.* **2017**, *67*, 443. [\[CrossRef\]](#)
- Ramesh, G.K.; Gireesha, B. Influence of heat source/sink on a Maxwell fluid over a stretching surface with convective boundary condition in the presence of nanoparticles. *Ain Shams Eng. J.* **2014**, *5*, 991–998. [\[CrossRef\]](#)
- Mehmood, R.; Nadeem, S.; Saleem, S.; Akbar, N.S. Flow and heat transfer analysis of Jeffery nano fluid impinging obliquely over a stretched plate. *J. Taiwan Inst. Chem. Eng.* **2017**, *74*, 49–58. [\[CrossRef\]](#)
- Kumar, K.G.; Ramesh, G.K.; Gireesha, B.; Gorla, R. Characteristics of Joule heating and viscous dissipation on three-dimensional flow of Oldroyd B nanofluid with thermal radiation. *Alex. Eng. J.* **2018**, *57*, 2139–2149. [\[CrossRef\]](#)
- Rana, S.; Mehmood, R.; Narayana, P.S.; Akbar, N. Free Convective Nonaligned Non-Newtonian Flow with Non-linear Thermal Radiation. *Commun. Theor. Phys.* **2016**, *66*, 687–693. [\[CrossRef\]](#)
- Awais, M.; Aqsa, Malik, M.; Awan, S.E. Generalized magnetic effects in a Sakiadis flow of polymeric nano-liquids: Analytic and numerical solutions. *J. Mol. Liq.* **2017**, *241*, 570–576. [\[CrossRef\]](#)
- Ahmed, N.; Khan, U.; Mohyud-Din, S.T. A theoretical investigation of unsteady thermally stratified flow of  $\gamma\text{Al}_2\text{O}_3$ –H<sub>2</sub>O and  $\gamma\text{Al}_2\text{O}_3$ –C<sub>2</sub>H<sub>6</sub>O<sub>2</sub> nanofluids through a thin slit. *J. Phys. Chem. Solids* **2018**, *119*, 296–308. [\[CrossRef\]](#)
- Phule, A.; Ram, S.; Shinde, S.; Choi, J.; Tyagi, A. Negative optical absorption and up-energy conversion in dendrites of nanostructured silver grafted with  $\alpha/\beta$ -poly(vinylidene fluoride) in small hierarchical structures. *J. Phys. Chem. Solids* **2018**, *115*, 254–264. [\[CrossRef\]](#)

25. Rana, S.; Mehmood, R.; Akbar, N.S. Mixed convective oblique flow of a Casson fluid with partial slip, internal heating and homogeneous–heterogeneous reactions. *J. Mol. Liq.* **2016**, *222*, 1010–1019. [[CrossRef](#)]
26. Iqbal, Z.; Mehmood, R.; Azhar, E.; Mehmood, Z. Impact of inclined magnetic field on micropolar Casson fluid using Keller box algorithm. *Eur. Phys. J. Plus* **2017**, *132*, 175. [[CrossRef](#)]
27. Tabassum, R.; Mehmood, R.; Nadeem, S. Impact of viscosity variation and micro rotation on oblique transport of Cu- water fluid. *J. Colloid Interface Sci.* **2017**, *501*, 304–310. [[CrossRef](#)]
28. Awais, M.; Hayat, T.; Muqaddass, N.; Ali, A.; Awan, S.E. Nanoparticles and nonlinear thermal radiation properties in the rheology of polymeric material. *Results Phys.* **2018**, *8*, 1038–1045. [[CrossRef](#)]
29. Dawar, A.; Wakif, A.; Thumma, T.; Shah, N.A. Towards a new MHD non-homogeneous convective nanofluid flow model for simulating a rotating inclined thin layer of sodium alginate-based iron oxide exposed to incident solar energy. *Int. Commun. Heat Mass Transfer.* **2022**, *130*, 105800. [[CrossRef](#)]
30. Siddiqa, S.; Naqvi, S.; Begum, N.; Awan, S.; Hossain, M. Thermal radiation therapy of biomagnetic fluid flow in the presence of localized magnetic field. *Int. J. Therm. Sci.* **2018**, *132*, 457–465. [[CrossRef](#)]
31. Awan, S.E.; Khan, Z.A.; Awais, M.; Rehman, S.U.; Raja, M.A.Z. Numerical treatment for hydro-magnetic unsteady channel flow of nanofluid with heat transfer. *Results Phys.* **2018**, *9*, 1543–1554. [[CrossRef](#)]
32. Mehmood, A.; Zameer, A.; Raja, M.A.Z. Intelligent computing to analyze the dynamics of Magnetohydrodynamic flow over stretchable rotating disk model. *Appl. Soft Comput.* **2018**, *67*, 8–28. [[CrossRef](#)]
33. Raja, M.A.Z.; Ahmed, T.; Shah, S.M. Intelligent computing strategy to analyze the dynamics of convective heat transfer in MHD slip flow over stretching surface involving carbon nanotubes. *J. Taiwan Inst. Chem. Eng.* **2017**, *80*, 935–953. [[CrossRef](#)]
34. Raja, M.A.Z.; Azad, S.; Shah, S.M. Bio-inspired computational heuristics to study the boundary layer flow of the Falkner-Scan system with mass transfer and wall stretching. *Appl. Soft Comput.* **2017**, *57*, 293–314. [[CrossRef](#)]
35. Raja, M.A.; Khan, M.A.; Mahmood, T.; Farooq, U.; Chaudhary, N.I. Design of bio-inspired computing technique for nanofluidics based on nonlinear Jeffery–Hamel flow equations. *Can. J. Phys.* **2016**, *94*, 474–489. [[CrossRef](#)]
36. Raja, M.A.Z.; Manzar, M.A.; Shah, F.H.; Shah, F.H. Intelligent computing for Mathieu’s systems for parameter excitation, vertically driven pendulum and dusty plasma models. *Appl. Soft Comput.* **2018**, *62*, 359–372. [[CrossRef](#)]
37. Barman, T.; Roy, S.; Chamkha, A.J. Magnetized Bi-convective Nanofluid Flow and Entropy Production Using Temperature-sensitive Base Fluid Properties: A Unique Approach. *J. Appl. Comput. Mech.* **2021**, *4*, 5. [[CrossRef](#)]
38. Koriko, O.K.; Shah, N.A.; Saleem, S.; Chung, J.D.; Omowaye, A.J.; Oreyni, T. Exploration of bioconvection flow of MHD thixotropic nanofluid past a vertical surface coexisting with both nanoparticles and gyrotactic microorganisms. *Sci. Rep.* **2021**, *11*, 16627. [[CrossRef](#)]
39. Rehman, S.; Zeeshan Rasheed, H.U.; Islam, S. Visualization of multiple slip effects on the hydromagnetic Casson nanofluid past a nonlinear extended permeable surface: A numerical approach. *Waves Random Complex Media* **2022**, *22*, 1–18.
40. Rasheed, H.U.; Islam, S.; Zeeshan Abbas, T.; Khan, J. Analytical treatment of MHD flow and chemically reactive Casson fluid with Joule heating and variable viscosity effect. *Waves Random Complex Media* **2022**, *5*, 1–17. [[CrossRef](#)]
41. Rasheed, H.U.; Khan, W.; Khan, I.; Alshammari, N.; Hamadneh, N. Numerical computation of 3D Brownian motion of thin film nanofluid flow of convective heat transfer over a stretchable rotating surface. *Sci. Rep.* **2022**, *12*, 2708.